ACS APPLIED MATERIALS & INTERFACES

Research Article

www.acsami.org

Carbon-Free Electrocatalyst for Oxygen Reduction and Oxygen Evolution Reactions

Yang Yang,[†,‡,1] Huilong Fei,[†] Gedeng Ruan,[†] Lei Li,[†] Gunuk Wang,[†,2] Nam Dong Kim,[†] and James M. Tour*[,†,‡,§]

[†]Department of Chemistry, [‡]Smalley Institute for Nanoscale Science and Technology, [§]Department of Materials Science and NanoEngineering, Rice University, 6100 Main Street, Houston, Texas 77005, United States

Supporting Information

ABSTRACT: A nanoporous Ag-embedded SnO_2 thin film was fabricated by anodic treatment of electrodeposited Ag−Sn alloy layers. The ordered nanoporous structure formed by anodization played a key role in enhancing the electrocatalytic performance of the Ag-embedded SnO_2 layer in several ways: (1) the roughness factor of the thin film is greatly increased from 23 in the compact layer to 145 in the nanoporous layer, creating additional active sites that are involved in oxygen electrochemical reactions; (2) a trace amount of Ag (~1.7 at %, corresponding to a Ag loading of ~3.8 μg cm^{-2}) embedded in the self-organized SnO_2 nanoporous matrix avoids the agglomeration of nanoparticles, which is a common problem leading to the electrocatalyst deactivation; (3) the fabricated nanoporous thin film is active without additional additives or porous carbon that is usually necessary to support and stabilize the electrocatalyst. More importantly, the Ag-embedded SnO_2 nanoporous thin film shows outstanding bifunctional oxygen electrochemical performance (oxygen reduction and evolution reactions) that is considered a promising candidate for use in metal-air batteries. The present technique has a wide range of applications for the preparation of other carbon-free electrocatalytic nanoporous films that could be useful for renewable energy production and storage applications.

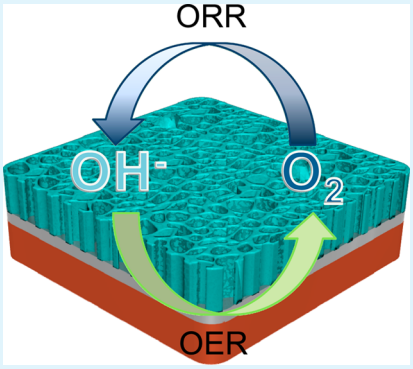

KEYWORDS: *nanoporous, silver-embedded tin oxide, SnO_2, bifunctional electrocatalysts, oxygen evolution reaction, oxygen reduction reaction*

INTRODUCTION

The metal-air battery (MAB) is a rapidly emerging technology that is regarded as the ultimate candidate to replace nonrenewable energy sources because of its extremely high energy density, comparable to gasoline.[1] In contrast to conventional rechargeable batteries, the active materials used in MABs have no direct reaction with the electrolytes and work as catalysts to reduce the energy barrier for oxygen reduction reaction (ORR) in discharging and oxygen evolution reaction (OER) in charging.[2] Primarily because of the sluggish kinetics induced by multistep proton-coupled electron-transfer processes (four-electron catalytic reactions) and complex reaction pathways (different intermediate products) involved in the oxygen electrochemistry of ORR and OER, it is challenging to find a bifunctional oxygen catalyst (BOC) with efficient electrocatalytic activities for both ORR and OER.[3] To date, some precious metals and their oxides such as Pt, IrO_2, and RuO_2 are reported and are considered to be the most efficient BOC.[4−6] In addition to their scarcity, RuO_2 is thermodynamically unstable while Pt and IrO_2 catalysts can easily agglomerate, resulting in physical characteristics that cause their bifunctional catalytic activities to markedly diminish with time.[7] Although some precious metal-free oxides have been developed for BOC, such as spinel Co_3O_4 and MnO_2,[8,9] their poor conductivity limits their practical applications. Most recently, various carbon nanostructures, such as graphene, have been combined with spinel oxides to enhance the conductivity of those composites. Further doping of Co_3O_4 or MnO_2 with N, B, or P can afford efficient ORR performance comparable to Pt.[10−13] Unfortunately, the carbon rapidly decays under anodic oxidizing conditions, which makes the oxygen electrode stability poor during the charge/discharge cycling in rechargeable MABs.[14]

To meet the requirements for MABs, bifunctional oxygen electrodes need to (1) have open gas diffusion pathways and hydrophilicity to an electrolyte;[15] (2) have catalysts that are well dispersed on a conductive high surface area (porous) matrix to avoid aggregation;[16] (3) have efficient catalytic activity, with materials of abundant availability and acceptable cost for mass production;[17] (4) have high surface area in contact with the electrolyte and O_2;[18] and (5) be carbon-free to avoid the oxidative decay.[19] This led us to consider fabricating BOCs from carbon-free porous thin films. To this end, anodization is well-recognized as a feasible approach to synthesize well-controlled porous metal oxide films without using any templates.[20,21] Our recent investigations revealed that

Received: June 3, 2015
Accepted: August 31, 2015
Published: August 31, 2015

ACS Publications © 2015 American Chemical Society

DOI: 10.1021/acsami.5b04887
ACS Appl. Mater. Interfaces 2015, 7, 20607−20611

the anodically formed pores within a small geometrical area create many more electrocatalytically active sites than their counterpart compact films.[22]

For some time, Ag has been considered as a possible replacement for Pt in electrocatalytic applications because of its high catalytic activity, high electrical conductivity, better stability, and longer lifetime. It is ~100× less expensive than Pt.[23−25] To generate more electrocatalytically active sites as well as to avoid catalyst deactivation because of aggregation, various nanostructured Ag particles and composites have been synthesized. For example, one-dimensional Ag nanowires with high aspect ratios are reported to have better electrocatalytic activity than Ag particles in alkaline media.[26] Also, 45 nm Ag nanocubes show higher electrocatalytic performance than Ag particles.[27] However, to prevent any side effects caused by adding porous carbon supports, porous Ag is preferred for use as a gas diffusion oxygen electrode.[28] Although, to date, several techniques have been studied to fabricate porous Ag, such as template-assisted electrodeposition and dealloying, it is still an enormous challenge to fabricate nanoscale interconnected porous Ag using those methods.[29,30] Even though facile fabrication techniques such as anodization can convert most metals into nanoporous structures, Ag is one of the exceptions.[31] To overcome this challenge, we designed a new fabrication procedure: electrodeposition of a Ag−Sn alloy film, followed by anodization treatment of the deposited alloy layer. Sn was chosen to form an alloy film with Ag because Sn can be converted to a nanoporous structure by anodization.[32,33] The nanoporous layer synthesized by this approach has several advantages: (1) the nanoscale pores have an average size of ~10 nm; (2) the nanopores are ordered and interconnected; and (3) only a trace amount of Ag is needed to be embedded into the SnO_2 matrix, thereby avoiding the aggregation of Ag and reducing the cost of the electrocatalyst. The fabricated nanoporous AgSn films show efficient electrocatalytic ORR and OER performances and can be used as candidates for MABs.

RESULTS AND DISCUSSION

The process for fabricating the Ag-embedded SnO_2 nanoporous layers (AgSn NPL) is shown schematically in Figure 1a (see Supporting Information for details): (1) electrochemically polished copper foils were used as substrates, followed by (2) electrodeposition of compact Ag−Sn alloy layers (Figures S1 and S2), and finally, (3) anodization treatment of the alloy layers to form the AgSn NPL. After anodization, a self-organized and ordered porous structure with an average pore size ~10 nm was observed in the scanning electron microscopy (SEM) images (Figure 1b). Transmission electron microscopy (TEM) analyses (Figure 1c and Supporting Figure S3) of the AgSn NPL also show well-crystallized and ordered pores with sizes ~10 nm. The lattice fringes, as indicated in the high-resolution TEM image (Figure 1c right), is ~0.35 nm and can be ascribed to SnO_2(110).[34] Moreover, TEM elemental mapping performed on the AgSn NPL (Figure 1f) shows a uniform distribution of Sn and Ag throughout the anodized material. The compositions and atomic ratio between Sn and Ag in the AgSn NPL were investigated by X-ray photoelectron spectroscopy (XPS) (Figure 2). The AgSn NPL is mainly composed of Sn, Ag, and O with Ag/Sn in a 1.7% atomic ratio, which corresponds to Ag loading of ~3.8 μg cm^{-2}. The XPS Ag 3d peak at 368.2 eV is ascribed to Ag rather than to Ag oxides.[35] The two peaks at 486.7 and 495.1 eV are attributable to Sn 3d spin−orbit peaks of SnO_2.[36] We used XPS to estimate

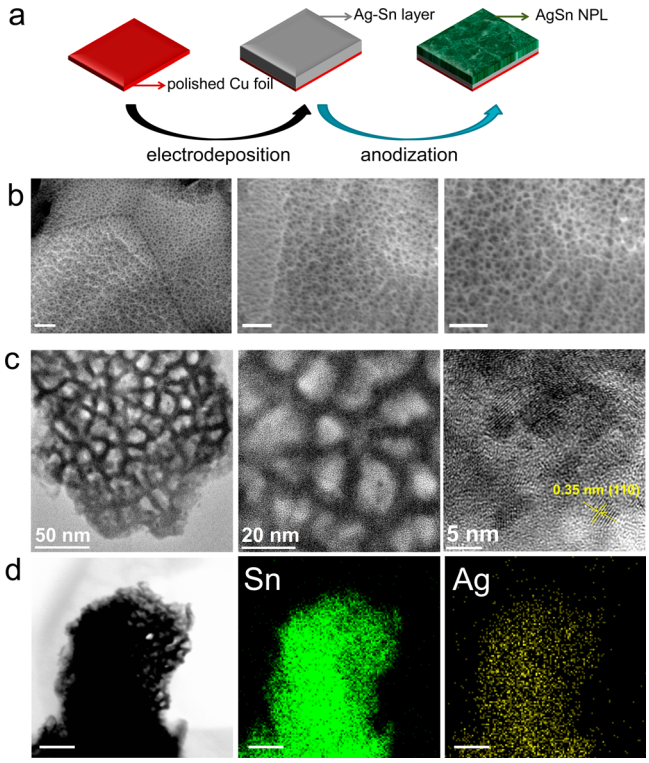

Figure 1. Schematic illustration of the fabrication processes and electron microscopy characterizations of the AgSn NPL. (a) Schematic illustration of the fabrication processes. (b) SEM images of the AgSn NPL with different magnifications. The scale bar in b denotes 100 nm. (c) TEM images of the AgSn NPL with different magnifications. The lattice fringes, as indicated in the high-resolution TEM image (right), is ~0.35 nm and can be ascribed to SnO_2(110). (d) TEM image and elemental mapping of the AgSn NPL. The scale bar in d denotes 50 nm.

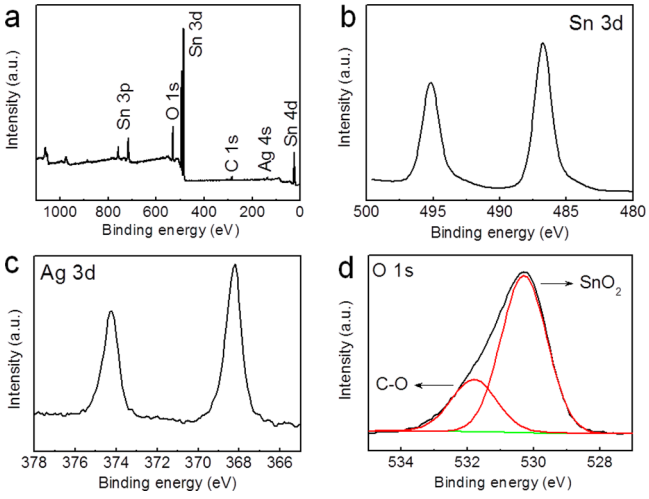

Figure 2. X-ray photoelectron spectra of the AgSn NPL. (a) Overview spectrum. (b) Sn 3d peak. (c) Ag 3d peak. (d) O 1s peak.

the Ag content in different samples such as the surface layer, the interior (bulk) layer composition of the AgSn NPL, and the as-deposited Ag−Sn layer as shown in the Supporting Table S1. The interior bulk of the sample was accessed by carefully scraping the surface with a knife before doing the XPS analysis. Those samples have similar Ag content (Supporting Figure S4), which indicates that anodization treatment has no effect on Ag

DOI: 10.1021/acsami.5b04887
ACS Appl. Mater. Interfaces 2015, 7, 20607−20611

content in the films. On the basis of this, the Ag/Sn ratio is controlled by adjusting the electrodeposition conditions, for example, the plating solution concentration. To demonstrate this assumption, we used a plating solution with lower Ag concentration to deposit the Ag−Sn layer. We find that the Ag content in the NPL decreases linearly (Supporting Table S2) with Ag salt concentration in the plating solution. The sample with less Ag content shows worse electrochemical performance (Supporting Figure S5). Considering the advantages of using extremely low loading mass of Ag, higher Ag content is not recommended because of cost concerns. Because of the high surface area of the AgSn NPL, the C−O bond from organic molecules absorbed in the pores is also detected from the fitted XPS O 1s peak.[37]

Roughness factor (RF) is an import parameter, defined as the ratio of the electrochemically active surface area (EASA) to the geometric surface area of the electrode, to evaluate the active sites that may be involved in the electrochemical reactions.[38] After forming the nanoporous structure, the RF of the catalyst increased to 145, >6 times higher than the as-deposited AgSn alloy layer (RF ∼ 23, for calculation details see Supporting Information). The greatly improved surface roughness produces more electrochemically active sites in the AgSn NPL. With more sites for electrocatalytic reactions, this material is superior to other nanostructured Ag catalysts.

The bifunctional electrocatalytic activity of the AgSn NPL as oxygen electrode was examined through testing cyclic voltammograms (CVs) and linear sweep voltammetry (LSV) in O_2-saturated 0.1 M aqueous NaOH with Hg/HgO (in 0.1 M NaOH) as the reference electrode. During the electrochemical testing, the AgSn NPL on Cu foil was used directly as the working electrode without adding any additives or conductive carbon. The representative CVs and LSV performed at a scan rate of 5 mV s^{-1} are shown in Figure 3 and Supporting Figure S6. To assess the ORR activity, a comparison between the CVs (Figure 3a) tested in O_2- and Ar-saturated 0.1 M NaOH was made. The AgSn NPL catalyst exhibited a symmetrical CV curve in Ar-saturated electrolyte. By contrast, a prominent catholic ORR peak with an onset potential (defined as the potential under which the reduction current is observed) of ∼0.87 V (vs RHE) was observed in O_2-saturated electrolyte.[39] The OER activity of the AgSn NPL investigated by CV (Supporting Figure S7) demonstrates pronounced oxygen evolution current. A pair of redox reaction peaks (represented by $Ag_2O + 2OH^- \leftrightarrows 2AgO + H_2O + 2e^-$), labeled as A2 (1.6 V vs RHE) and C2 (1.3 V vs RHE) in Figure 3b, is attributed to the formation and reduction of AgO, respectively.[40] Figure 3b also shows the complete electrocatalytic reactions (ORR and OER) and redox reactions (oxidation of Ag and reduction of silver oxides). An additional pair of redox reaction peaks (represented by $2Ag + 2OH^- \leftrightarrows Ag_2O + H_2O + 2e^-$) at 1.28 V (vs RHE, A1) and 0.96 V (vs RHE, C1) is ascribed to the formation and reduction of Ag_2O, respectively, whereas the presence of a shoulder (1.22 V vs RHE) close to A1 is ascribable to the AgOH intermediates.[41] The silver oxides formed during the anodic scan are recognized as OER active materials in the nanoporous layer. Moreover, the high ORR activity is also evident from the electron-transfer number (n, the number of electrons exchanged per oxygen molecule for the ORR) and the kinetic current density (J_k) obtained on the basis of the Koutecky−Levich (K-L) eqs (Supporting Information).[42] To do this, LSV obtained by rotating disc electrode (RDE) analysis (Figure 3c) of the catalyst with electrode rotation rates from 400 to 1600 rpm was investigated. Therefore, the corresponding K-L plots (J^{-1} vs $\omega^{-1/2}$) were then obtained at various potentials. The n was determined to be ∼3.1 at different potentials, demonstrating that the AgSn NPL was mainly dominated by a four-electron transfer pathway (with oxygen being directly reduced to water). To our knowledge, many carbon-supported Ag catalysts have two-electron transfer dominated ORR pathways producing H_2O_2 that is further reduced to water by two more electrons. These are commonly encountered when using carbon as the conductive substrate.[43] This complicated substrate issue is caused by the two-electron transfer ORR process on the carbon surfaces. In the present work, by embedding Ag into the self-organized SnO_2 nanoporous layer, the catalytic activity is enhanced by avoiding the influence of carbon substrates. Moreover, the J_k is determined to be 1.54 mA cm^{-2} at 0.4 V (vs RHE). The bifunctional oxygen electrode activity of the AgSn NPL (porous thin film) is also demonstrated by LSV (Figure 3d) obtained through RDE analysis at 900 rpm. As expected, cathodic current for ORR and anodic current for OER are observed.

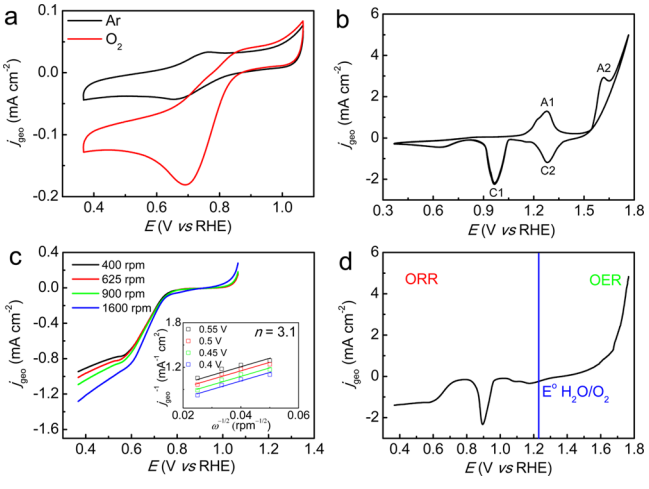

Figure 3. Bifunctional electrocatalytic performance of the AgSn NPL as oxygen electrode measured at scan rate of 5 mV s^{-1}. (a) ORR performance tested by CV in Ar (black line) and O_2 (red line). (b) CV tested in a wide potential range to demonstrate the ORR and OER performance. (c) LSV tested by rotating disk electrode at rotation rates from 400 to 1600 rpm shows the ORR performance. The inset in c is Koutecky−Levich (K-L) plots at different overpotentials. (d) LSV performed at 900 rpm shows bifunctional ORR and OER performance.

To demonstrate the advantages of the nanoporous structure in the AgSn NPL (porous thin film), control experiments were performed by CV analysis of the as-deposited Sn−Ag alloy layer (compact film) and porous SnO_2 (porous thin film) in O_2-saturated 0.1 M NaOH (Supporting Figure S8). The porous SnO_2 layer has sluggish oxygen electrochemistry, and no distinguished ORR or OER current can be observed, which would not have any negative effects on the catalytic activity of Ag, unlike carbon supports. Even though the as-deposited Ag−Sn compact alloy layer delivers some oxygen electrode catalytic activity, the observed ORR and OER currents are ∼50% and ∼80%, respectively, less than the AgSn NPL. The high performance of the AgSn NPL is attributed to the greater number of electrochemically active sites for catalytic reactions, to the open channels for molecular transport created by the

DOI: 10.1021/acsami.5b04887
ACS Appl. Mater. Interfaces 2015, 7, 20607−20611

formation of the self-organized nanoporous structure, and to the well-dispersed Ag in the porous layer. We also tested the CV of the AgSn NPL for 2000 cycles, and we found increased catalytic currents in both ORR and OER (Supporting Figure S9). This means that the porous layer goes through a gradual activation of the interior layer during the cycling test and demonstrates good performance for long-term utilization without decay. Despite the extremely low Ag loading (~3.8 $\mu g\ cm^{-2}$, which is equal to 280 $\mu g\ cm^{-2}$ calculated on the basis of the entire film), the catalytic activity of the AgSn NPL is better than most state-of-the-art nanostructured Ag, Ag-based alloy and Ag composites (for detailed comparison, see Supporting Table S3), and can be considered as a competitive candidate for use as bifunctional oxygen electrodes in MABs.

CONCLUSION

In summary, we demonstrated a facile approach to fabricate bifunctional oxygen electrodes with low concentrations of Ag embedded in SnO_2 nanoporous layers. After forming the highly porous structure, the roughness factor of the catalyst was greatly improved to provide more electrocatalytically active sites for ORR and OER and open pathways for transport of gas molecules. The synthesized AgSn NPL is a carbon- and additive-free catalyst that could be used in MABs, which can resolve the poor cyclability problem raised by the side reactions of carbon in the common carbon-containing oxygen electrodes.

ASSOCIATED CONTENT

Supporting Information

. The Supporting Information is available free of charge on the ACS Publications website at DOI: 10.1021/acsami.5b04887.

Experimental procedures, characterization methodology, electrochemical measurements, SEM, XRD, TEM, and XPS spectra (PDF)

AUTHOR INFORMATION

Corresponding Author

*E-mail: tour@rice.edu.

Present Addresses

[1]NanoScience Technology Center, University of Central Florida, 12424 Research Parkway Suite 400, Orlando, Florida 32826, USA.

[2]KU-KIST Graduate School of Converging Science and Technology, Korea University, Seoul 136-701, Korea.

Notes

The authors declare no competing financial interest.

ACKNOWLEDGMENTS

We thank the Peter M. and Ruth L. Nicholas Post-Doctoral Fellowship of the Smalley Institute for Nanoscale Science and Technology for financial support (Y. Yang). Additional funding was provided by the AFOSR (FA9550-14-1-0111).

REFERENCES

(1) Girishkumar, G.; McCloskey, B.; Luntz, A. C.; Swanson, S.; Wilcke, W. Lithium-Air Battery: Promise and Challenges. *J. Phys. Chem. Lett.* **2010**, *1*, 2193−2203.

(2) Zhang, T.; Zhou, H. A Reversible Long-Life Lithium-Air Battery in Ambient Air. *Nat. Commun.* **2013**, *4*, 1817.

(3) Sasikala, N.; Ramya, K.; Dhathathreyan, K. S. Bifunctional Electrocatalyst for Oxygen/Air Electrodes. *Energy Convers. Manage.* **2014**, *77*, 545−549.

(4) Lu, Y. C.; Xu, Z.; Gasteiger, H. A.; Chen, S.; Hamad-Schifferli, K.; Yang, S. H. Platinum-Gold Nanoparticles: A Highly Active Bifunctional Electrocatalyst for Rechargeable Lithium-Air Batteries. *J. Am. Chem. Soc.* **2010**, *132*, 12170−12171.

(5) Kong, F. D.; Zhang, S.; Yin, G. P.; Zhang, N.; Wang, Z. B.; Du, C. Y. Preparation of $Pt/Ir_x(IrO_2)_{10-x}$ Bifunctional Oxygen Catalyst for Unitized Regenerative Fuel Cell. *J. Power Sources* **2012**, *210*, 321−326.

(6) Jian, Z.; Liu, P.; Li, F.; He, P.; Guo, X.; Chen, M.; Zhou, H. Core-Shell-Structured CNT@RuO2 Composite as a High-Performance Cathode Catalyst for Rechargeable Li-O_2 Batteries. *Angew. Chem., Int. Ed.* **2014**, *53*, 442−446.

(7) Gorlin, Y.; Jaramillo, T. F. A Bifunctional Nonprecious Metal Catalyst for Oxygen Reduction and Water Oxidation. *J. Am. Chem. Soc.* **2010**, *132*, 13612−13614.

(8) Ryu, W. H.; Yoon, T. H.; Song, S. H.; Jeon, S.; Park, Y. J.; Kim, I. D. Bifunctional Composite Catalysts Using Co_3O_4 Nanofibers Immobilized on Nonoxidized Graphene Nanoflakes for High-Capacity and Long-Cycle Li-O_2 Batteries. *Nano Lett.* **2013**, *13*, 4190−4197.

(9) Meng, Y.; Song, W.; Huang, H.; Ren, Z.; Chen, S. Y.; Suib, S. L. Structure-Property Relationship of Bifunctional MnO_2 Nanostructures: Highly Efficient, Ultra-Stable Electrochemical Water Oxidation and Oxygen Reduction Reaction Catalysts Identified in Alkaline Media. *J. Am. Chem. Soc.* **2014**, *136*, 11452−11464.

(10) Liang, Y.; Li, Y.; Wang, H.; Zhou, J.; Wang, J.; Regier, T.; Dai, H. Co_3O_4 Nanocrystals on Graphene as A Synergistic Catalyst for Oxygen Reduction Reaction. *Nat. Mater.* **2011**, *10*, 780−786.

(11) Wu, Z. S.; Yang, S.; Sun, Y.; Parvez, K.; Feng, X.; Müllen, K. 3D Nitrogen-Doped Graphene Aerogel-Supported Fe_3O_4 Nanoparticles as Efficient Electrocatalysts for the Oxygen Reduction Reaction. *J. Am. Chem. Soc.* **2012**, *134*, 9082−9085.

(12) Wang, S.; Zhang, L.; Xia, Z.; Roy, A.; Chang, D. K.; Baek, J. B.; Dai1, L. BCN Graphene as Efficient Metal-Free Electrocatalyst for the Oxygen Reduction Reaction. *Angew. Chem., Int. Ed.* **2012**, *51*, 4209−4212.

(13) Li, Y.; Zhou, W.; Wang, H.; Xie, L.; Liang, Y.; Wei, F.; Idrobo, J. C.; Pennycook, S. J.; Dai, H. An Oxygen Reduction Electrocatalyst Based on Carbon Nanotube-Graphene Complexes. *Nat. Nanotechnol.* **2012**, *7*, 394−400.

(14) Li, F.; Tang, D. M.; Chen, Y.; Golberg, D.; Kitaura, H.; Zhang, T.; Yamada, A.; Zhou, H. Ru/ITO: A Carbon-Free Cathode for Nonaqueous Li-O_2 Battery. *Nano Lett.* **2013**, *13*, 4702−4707.

(15) Lee, J. S.; Kim, S. T.; Cao, R.; Choi, N. S.; Liu, M.; Lee, K. T.; Cho, J. Metal-Air Batteries with High Energy Density: Li-Air versus Zn-Air. *Adv. Energy Mater.* **2011**, *1*, 34−50.

(16) Black, R.; Oh, S. H.; Lee, J. H.; Yim, T.; Adams, B.; Nazar, L. F. Screening for Superoxide Reactivity in Li-O_2 Batteries: Effect on Li_2O_2/LiOH Crystallization. *J. Am. Chem. Soc.* **2012**, *134*, 2902−2905.

(17) Jung, H. G.; Hassoun, J.; Park, J. B.; Sun, Y. K.; Scrosati, B. An Improved High-Performance Lithium-Air Battery. *Nat. Chem.* **2012**, *4*, 579−585.

(18) Girishkumar, G.; McCloskey, B.; Luntz, A. C.; Swanson, S.; Wilcke, W. Lithium-Air Battery: Promise and Challenges. *J. Phys. Chem. Lett.* **2010**, *1*, 2193−2203.

(19) Wei, J.; Ng, D.; Tang, M.; Jaramillo, T. F. A Carbon-Free, Precious-Metal-Free, High-Performance O_2 Electrode for Regenerative Fuel Cells and Metal-Air Batteries. *Energy Environ. Sci.* **2014**, *7*, 2017−2024.

(20) Yang, Y.; Albu, S. P.; Kim, D.; Schmuki, P. Enabling the Anodic Growth of Highly Ordered V_2O_5 Nanoporous/Nanotubular Structures. *Angew. Chem., Int. Ed.* **2011**, *50*, 9071−9075.

(21) Yang, Y.; Ruan, G.; Xiang, C.; Wang, G.; Tour, J. M. Flexible Three-Dimensional Nanoporous Metal-Based Energy Devices. *J. Am. Chem. Soc.* **2014**, *136*, 6187−6190.

(22) Yang, Y.; Fei, H.; Ruan, G.; Xiang, C.; Tour, J. M. Efficient Electrocatalytic Oxygen Evolution on Amorphous Nickel-Cobalt Binary Oxide Nanoporous Layers. *ACS Nano* **2014**, *8*, 9518−9523.

(23) Hsieh, C. T.; Pan, C.; Chen, W. Y. Synthesis of Silver Nanoparticles on Carbon Papers for Electrochemical Catalysts. *J. Power Sources* **2011**, *196*, 6055−6061.

DOI: 10.1021/acsami.5b04887
ACS Appl. Mater. Interfaces 2015, 7, 20607−20611

(24) Lu, Q.; Rosen, J.; Zhou, Y.; Hutchings, G. S.; Kimmel, Y. C.; Chen, J. G.; Jiao, F. A Selective and Efficient Electrocatalyst for Carbon Dioxide Reduction. *Nat. Commun.* **2014**, *5*, 3242.
(25) Wen, C.; Yin, A.; Dai, W. L. Recent Advances in Silver-Based Heterogeneous Catalysts for Green Chemistry Processes. *Appl. Catal., B* **2014**, *160−161*, 730−741.
(26) Kim, B.; Choi, Y.; Cho, S. Y.; Yun, Y. S.; Jin, H. J. Silver Nanowire Catalysts on Carbon Nanotubes-Incorporated Bacterial Cellulose Membrane Electrodes for Oxygen Reduction Reaction. *J. Nanosci. Nanotechnol.* **2013**, *13*, 7454−7458.
(27) Lee, C. L.; Tsai, Y. L.; Huang, C. H.; Huang, K. L. Performance of Silver Nanocubes Based on Electrochemical Surface Area for Catalyzing Oxygen Reduction Reaction. *Electrochem. Commun.* **2013**, *29*, 37−40.
(28) Lee, M. N.; Mohraz, A. Hierarchically Porous Silver Monoliths from Colloidal Bicontinuous Interfacially Jammed Emulsion Gels. *J. Am. Chem. Soc.* **2011**, *133*, 6945−6947.
(29) Cherevko, S.; Xing, X.; Chung, C. H. Electrodeposition of Three-Dimensional Porous Silver Foams. *Electrochem. Commun.* **2010**, *12*, 467−470.
(30) Wan, D.; Xia, X.; Wang, Y.; Xia, Y. Robust Synthesis of Gold Cubic Nanoframes through a Combination of Galvanic Replacement, Gold Deposition, and Silver Dealloying. *Small* **2013**, *9*, 3111−3117.
(31) Yang, Y.; Lee, K.; Zobel, M.; Maćković, M.; Unruh, T.; Spiecker, E.; Schmuki, P. Formation of Highly Ordered VO_2 Nanotubular/Nanoporous Layers and Their Supercooling Effect in Phase Transitions. *Adv. Mater.* **2012**, *24*, 1571−1575.
(32) Fujiwara, Y.; Kobayashi, Y.; Higuchi, N.; Hoshiyama, Y.; Miyake, H. Codeposition Mechanism in Sn/Ag Nanoparticle Composite Plating. *Electrochim. Acta* **2013**, *89*, 623−630.
(33) Shin, H. C.; Dong, J.; Liu, M. Porous Tin Oxides Prepared Using an Anodic Oxidation Process. *Adv. Mater.* **2004**, *16*, 237−240.
(34) Zeng, W.; Liu, T.; Wang, Z. Enhanced Gas Sensing Properties by SnO_2 Nanosphere Functionalized TiO_2 Nanobelts. *J. Mater. Chem.* **2012**, *22*, 3544−3548.
(35) Zou, M.; Du, M.; Zhu, H.; Xu, C.; Fu, Y. Green Synthesis of Halloysite Nanotubes Supported Ag Nanoparticles for Photocatalytic Decomposition of Methylene Blue. *J. Phys. D: Appl. Phys.* **2012**, *45*, 325302.
(36) Wang, J. J.; Lv, A. F.; Wang, Y. Q.; Cui, B.; Yan, H. J.; Hu, J. S.; Hu, W. P.; Guo, Y. G.; Wan, L. J. Integrated Prototype Nanodevices via SnO_2 Nanoparticles Decorated SnSe Nanosheets. *Sci. Rep.* **2013**, *3*, 2613.
(37) Hopster, H.; Brundle, C. R. Use of SIMS for Studies of Adsorption on Well-Defined Metal Surfaces (1) Combined XPS/LEED/SIMS Studies of O_2, CO, H_2O, and H_2 on Ni (100). *J. Vac. Sci. Technol.* **1979**, *16*, 548−551.
(38) Law, M.; Greene, L. E.; Johnson, J. C.; Saykally, R.; Yang, P. Nanowire Dye-Sensitized Solar Cells. *Nat. Mater.* **2005**, *4*, 455−459.
(39) Takasu, Y.; Yoshinaga, N.; Sugimoto, W. Oxygen Reduction Behavior of RuO_2/Ti, IrO_2/Ti and Ir*M* (*M*: Ru, Mo, W, V) O_x/Ti Binary Oxide Electrodes in a Sulfuric Acid Solution. *Electrochem. Commun.* **2008**, *10*, 668−672.
(40) Innocenti, M.; Zafferoni, C.; Lavacchi, A.; Becucci, L.; Di Benedetto, F.; Carretti, E.; Vizza, F.; Foresti, M. L. Electroactivation of Microparticles of Silver on Glassy Carbon for Oxygen Reduction and Oxidation Reactions. *J. Electrochem. Soc.* **2014**, *161*, D3018−D3024.
(41) Guo, J.; Hsu, A.; Chu, D.; Chen, R. Improving Oxygen Reduction Reaction Activities on Carbon-Supported Ag Nanoparticles in Alkaline Solutions. *J. Phys. Chem. C* **2010**, *114*, 4324−4330.
(42) Treimer, S.; Tang, A.; Johnson, D. C. A Consideration of the Application of Koutecky-Levich Plots in the Diagnoses of Charge-Transfer Mechanisms at Rotated Disk Electrodes. *Electroanalysis* **2002**, *14*, 165−171.
(43) Garcia, A. C.; Gasparotto, L. H. S.; Gomes, J. F.; Tremiliosi-Filho, G. Straightforward Synthesis of Carbon-Supported Ag Nanoparticles and Their Application for the Oxygen Reduction Reaction. *Electrocatalysis* **2012**, *3*, 147−152.

DOI: 10.1021/acsami.5b04887
ACS Appl. Mater. Interfaces 2015, 7, 20607−20611